

Supplementary Discussion:

Strain rate near the tip of a rupture front

1- Subshear rupture

We discuss the maximum strain rate that can be obtained near a mode II rupture front. As we want to get the maximum strain rate, we consider a pure elastic case, not taking into account the viscoelastic behaviour inside the process zone at the fracture tip.

The stress at a distance y_0 from the fault core is computed in a 2D model within a referential frame moving with the rupture tip. There is a directivity effect that can be interpreted as a “relativistic contraction”, where the following parameters appear:

$$\alpha_d = \sqrt{1 - \frac{v^2}{c_d^2}} \quad \alpha_s = \sqrt{1 - \frac{v^2}{c_s^2}}.$$

c_d is the dilatational wave speed along the (x,y) plan and c_s is the shear wave speed. Independent of the choice of the boundary conditions, we have

$$c_s = \sqrt{\frac{\mu}{\rho}}$$

where μ is the shear modulus, and ρ is the density. On the other hand, c_d depends on the boundary conditions. For plane stress, we get

$$c_d = \sqrt{\frac{2}{1-\nu}} c_s,$$

(ν is the Poisson ratio) while for plane strain, we get

$$c_d = \sqrt{\frac{2(1-\nu)}{1-2\nu}} c_s.$$

with the coordinates of this moving frame ($\eta=x-vt$, $\xi=y_0$), one can define reduced coordinates for both dilatational and shear waves. In polar coordinates ($r_d = \gamma_d r$, θ_d):

$$\gamma_d r e^{i\theta_d} = \eta + i\alpha_d \zeta$$

$$\gamma_s r e^{i\theta_s} = \eta + i\alpha_s \zeta$$

As we are interested in distances ($\sim 100\text{m}$) small relative to the rupture size (several 10s of kilometres for large earthquakes), we use a Taylor expansion in powers of r , where r is the distance from the fracture.

Freund²² gives the first order **expression**, which is singular in $1/r^{1/2}$:

$$\sigma_{xx} = \frac{K_{II}}{\sqrt{2\pi r D}} \left[-2\alpha_s(1+2\alpha_d^2-\alpha_s^2) \frac{\sin(\frac{1}{2}\theta_d)}{\sqrt{\gamma_d}} + 2\alpha_s(1+\alpha_s^2) \frac{\sin(\frac{1}{2}\theta_s)}{\sqrt{\gamma_s}} \right]$$

$$\sigma_{yy} = \frac{K_{II}}{\sqrt{2\pi r D}} \left[2\alpha_s(1+\alpha_s^2) \frac{\sin(\frac{1}{2}\theta_d)}{\sqrt{\gamma_d}} - 2\alpha_s(1+\alpha_s^2) \frac{\sin(\frac{1}{2}\theta_s)}{\sqrt{\gamma_s}} \right]$$

$$\sigma_{xy} = \frac{K_{II}}{\sqrt{2\pi r D}} \left[4\alpha_d\alpha_s \frac{\cos(\frac{1}{2}\theta_d)}{\sqrt{\gamma_d}} - (1+\alpha_s^2) \frac{\cos(\frac{1}{2}\theta_s)}{\sqrt{\gamma_s}} \right]$$

This expression depends only on the instantaneous value of the stress intensity factor K_{II} , not on its time derivatives. The current rupture front speed **contributes to** several parameters: α_d, α_s, r and $D = 4\alpha_d\alpha_s - (1+\alpha_s^2)^2$. These parameters are defined while $D > 0$ and $0 < v < c_s < c_d$, or equivalently $v < c_R$, where c_R is the Rayleigh speed, which is the non-null rupture velocity that satisfies $D = 0$.

Supposing plane strain conditions ($\varepsilon_{zz} = 0$)

$$\varepsilon_{xx} = \frac{1-\nu^2}{E} \sigma_{xx} - \frac{\nu(1+\nu)}{E} \sigma_{yy}$$

$$\varepsilon_{yy} = -\frac{\nu(1+\nu)}{E} \sigma_{xx} + \frac{1-\nu^2}{E} \sigma_{yy}$$

$$\varepsilon_{xy} = \frac{1}{2\mu} \sigma_{xy}$$

Supposing plane stress condition ($\sigma_{zz} = 0$)

$$\varepsilon_{xx} = \frac{1}{E} (\sigma_{xx} - \nu\sigma_{yy})$$

$$\varepsilon_{yy} = \frac{1}{E} (\sigma_{yy} - \nu\sigma_{xx})$$

$$\varepsilon_{xy} = \frac{1}{2\mu} \sigma_{xy}$$

We get therefore the following expression for the volumetric strain $\Delta = \varepsilon_{xx} + \varepsilon_{yy} + \varepsilon_{zz}$:

$$\Delta = \frac{(1+\nu)(1-2\nu)}{E} \frac{2K_{II}}{\sqrt{2\pi r}D} \alpha_s (\alpha_s^2 - \alpha_d^2) \frac{\sin \frac{\theta_d}{2}}{\sqrt{\gamma_d}} \quad (\text{plane strain})$$

$$\Delta = \frac{1-\nu}{E} \frac{2K_{II}}{\sqrt{2\pi r}D} \alpha_s (\alpha_s^2 - \alpha_d^2) \frac{\sin \frac{\theta_d}{2}}{\sqrt{\gamma_d}} \quad (\text{plane stress})$$

We can then deduce the time derivative of volumetric strain. Supposing that the rupture tip propagates at a constant speed v , the time dependence lies in the spatial terms r , γ_i and θ_i . We get

$$\frac{d\Delta}{dt} = \frac{(1+\nu)(1-2\nu)}{E} \frac{2K_{II}}{\sqrt{2\pi D}} \alpha_s (\alpha_s^2 - \alpha_d^2) v \frac{\sin(\frac{3\theta_d}{2})}{(\gamma_d r)^{3/2}} \quad (\text{plane strain})$$

$$\frac{d\Delta}{dt} = \frac{1-\nu}{E} \frac{2K_{II}}{\sqrt{2\pi D}} \alpha_s (\alpha_s^2 - \alpha_d^2) v \frac{\sin(\frac{3\theta_d}{2})}{(\gamma_d r)^{3/2}} \quad (\text{plane stress})$$

The strain rate scales as $1/r^{3/2}$. Dewers and Reches⁷ computed strain rate 3 mm away from the fault and reach strain rate as large as $10^6/s$. If we made the same computation farther from the fault (100 m), a subshear rupture would provide a strain rate of $10^{-8}/s$ only.

In the four equations above, there is the same constant $\frac{k}{E} \frac{2K_{II}}{\sqrt{2\pi D}} \alpha_s (\alpha_s^2 - \alpha_d^2) v$, with $k = (1+\nu)(1-2\nu)$

or $k = 1-\nu$. The time dependence is present only through the location terms $r, \gamma_d, \theta, \theta_d$. The constant involve the stress intensity factor K_{II} , which is poorly known. The preservation of the initial structure of the rock requires it underwent only small strain. Therefore, we chose to normalize both Δ and $\partial\Delta/\partial t$ so that the maximum strain is 2%, to assess what maximum strain rate is reachable with this small strain condition. We plot $\partial\Delta/\partial t$ versus Δ in figure 4 of the main text.

We get also the maximum shear strain in the (x,y) plane as $\varepsilon_s = \sqrt{\left(\frac{\varepsilon_{xx} - \varepsilon_{yy}}{2}\right)^2 + \varepsilon_{xy}^2}$.

$$\varepsilon_s = \frac{1}{2\mu} \frac{K_{II}}{\sqrt{2\pi D}} \sqrt{\left(4\alpha_d \alpha_s \frac{\cos\left(\frac{\theta_d}{2}\right)}{\sqrt{\gamma_d r}} - (1+\alpha_s^2) \frac{\cos\left(\frac{\theta_s}{2}\right)}{\sqrt{\gamma_s r}}\right)^2 + 4\alpha_s^2 \left((1+\alpha_d^2) \frac{\sin\left(\frac{\theta_d}{2}\right)}{\sqrt{\gamma_d r}} - (1+\alpha_s^2) \frac{\sin\left(\frac{\theta_s}{2}\right)}{\sqrt{\gamma_s r}} \right)^2} \quad (\text{plane strain})$$

Its time derivative can be computed analytically, but this large expression is cumbersome, so that we computed it with finite differences.

Higher order terms.

We now discuss the higher order terms in the asymptotic expansion.

The next term of the development is the T stress, which is uniform and induces also a uniform strain.

Hence, the time derivative of strain is null.

The next terms of the stress and strain development are terms proportional to $r^{1/2+n}$, with n being an integer.

The order of magnitude of the strain rate can be computed with $\frac{d\varepsilon}{dt} \cong \frac{d\varepsilon}{dr} \frac{dr}{dt} \cong v_{rupt} \frac{d\varepsilon}{dr}$, by remembering

that $r = \sqrt{(x - vt)^2 + y_0^2}$. Therefore, if a strain scales as $\varepsilon = r^n$, its time derivative scales as

$\dot{\varepsilon} = v_{rupt} \times r^{n-1} = \frac{v_{rupt}}{r} \varepsilon$. If we limit the strain to 2%, a rupture speed of 5000 m/s and a distance to the

fault equal to $y_0=100\text{m}$, the maximum strain rate is of the order of 1/s, about 100 times smaller than the experimental threshold for the transition to single fracturing to pulverization.

2- Supershear rupture

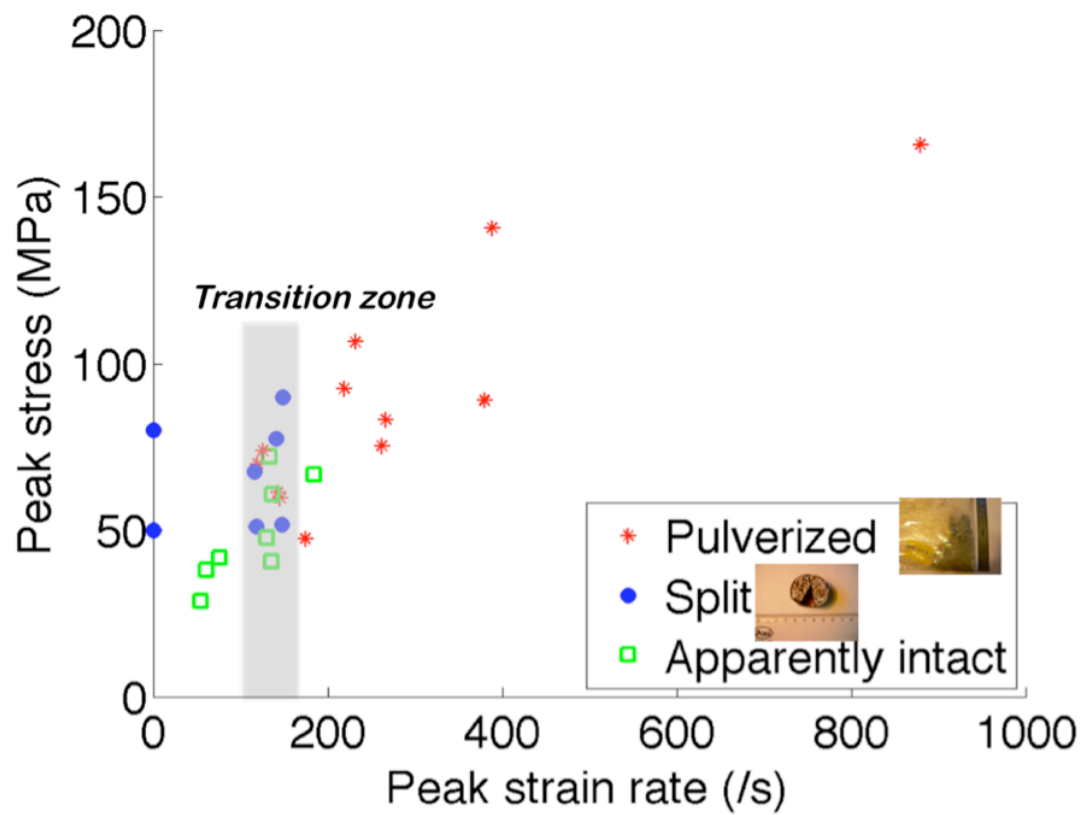
The previous development on subshear was made without process zone, poorly known for earthquakes.

To get insights on the stress generated by a supershear rupture, we have computed an asymptotic formulation of equations A4 of Samudrala and Rosakis²⁹, supposing the length of the process zone L is small.

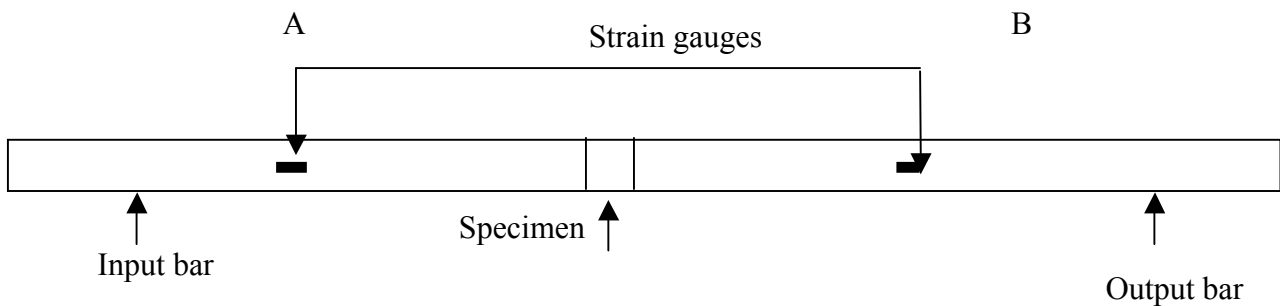
$$\begin{aligned} \sigma_{xx} &= \sqrt{\frac{\pi}{2}} \frac{K_{II}}{2} \frac{\sin(q\pi)}{q\pi} \left[\frac{(1 + 2\alpha_d^2 - \hat{\alpha}_s^2) \sin(q\theta_d)}{2\alpha_d (r/L)^q} + \frac{(1 - \hat{\alpha}_s^2)}{2\alpha_d} \frac{\sin(q\pi)}{\left(\frac{-\eta_1 - \hat{\alpha}_s \eta_2}{L}\right)^q} H(-\eta_1 - \hat{\alpha}_s \eta_2) \right] \\ \sigma_{yy} &= \sqrt{\frac{\pi}{2}} \frac{K_{II}}{2} \frac{\sin(q\pi)}{q\pi} \left[\frac{(1 - \hat{\alpha}_s^2)}{2\alpha_d} \frac{\sin(q\theta_d)}{(r/L)^q} - \frac{(1 - \hat{\alpha}_s^2)}{2\alpha_d} \frac{\sin(q\pi)}{\left(\frac{-\eta_1 - \hat{\alpha}_s \eta_2}{L}\right)^q} H(-\eta_1 - \hat{\alpha}_s \eta_2) \right] \\ \sigma_{xy} &= \sqrt{\frac{\pi}{2}} \frac{K_{II}}{2} \frac{\sin(q\pi)}{q\pi} \left[\frac{\cos(q\theta_d)}{(r/L)^q} - \frac{\cos(q\pi)}{\left(\frac{-\eta_1 - \hat{\alpha}_s \eta_2}{L}\right)^q} H(-\eta_1 - \hat{\alpha}_s \eta_2) \right] \end{aligned}$$

with $q = \frac{1}{\pi} \arctan \left(\frac{4 \alpha_d \hat{\alpha}_s}{(1 - \hat{\alpha}_s^2)^2} \right)$ and $\hat{\alpha}_s = \sqrt{\left(\frac{v^2}{c_s^2} \right)} - 1$. q lies between 0 and $\frac{1}{2}$. As stress decays as $1/r^q$,

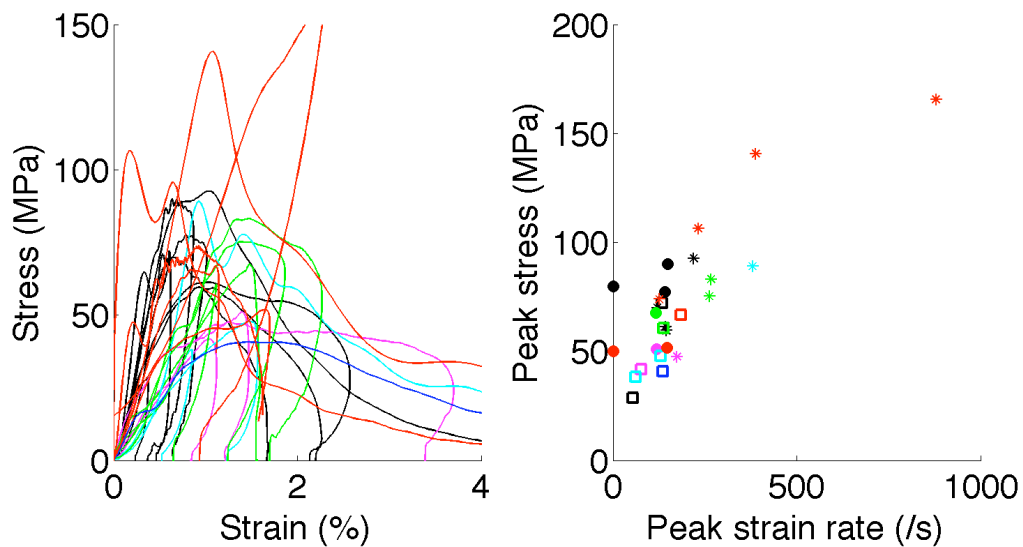
instead of $1/r^{1/2}$, supershear stress wave propagates farther. Stresses increase as a Heaviside step function, whose derivative is a Dirac delta function, giving a theoretically infinite pulse in strain rate.



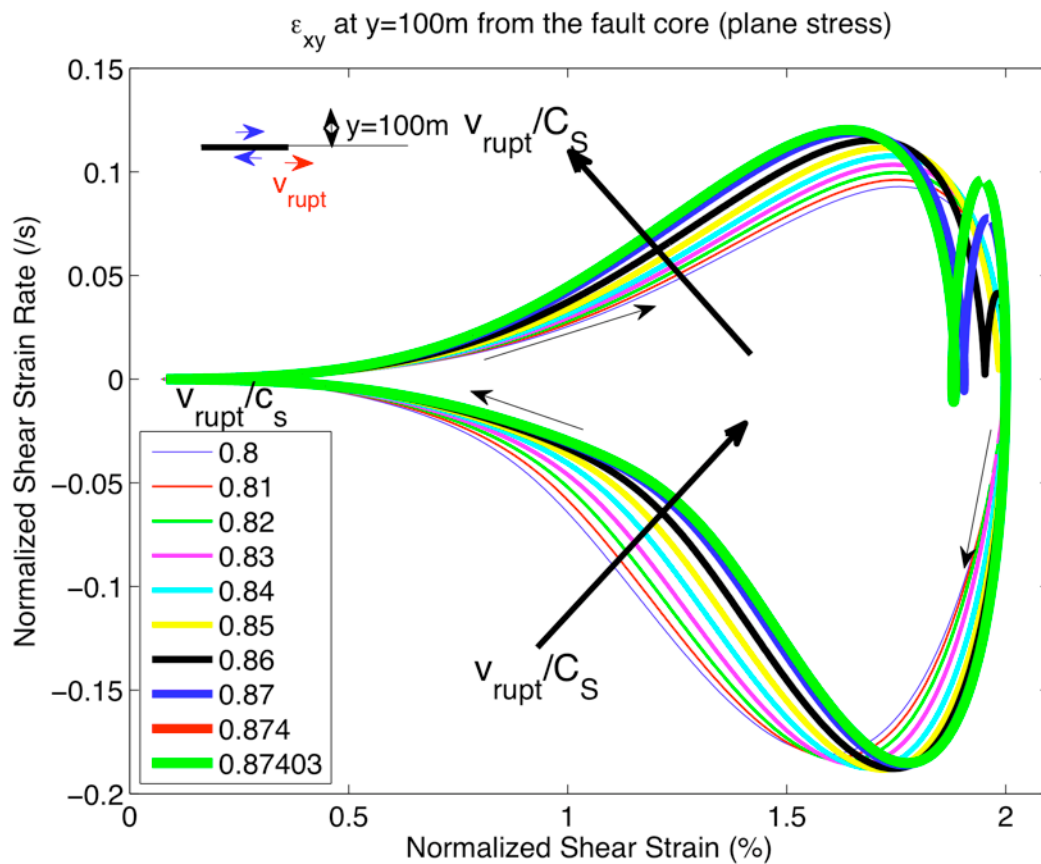
Supplementary Figure 1. Summary of the main findings of this paper. We show that rocks from the San Andreas Fault are pulverized if they are loaded at a rate larger than 150/s. Such high strain rate are not easy to obtain with a subshear earthquake, but may be reached in the Mach cone of a supershear earthquake.



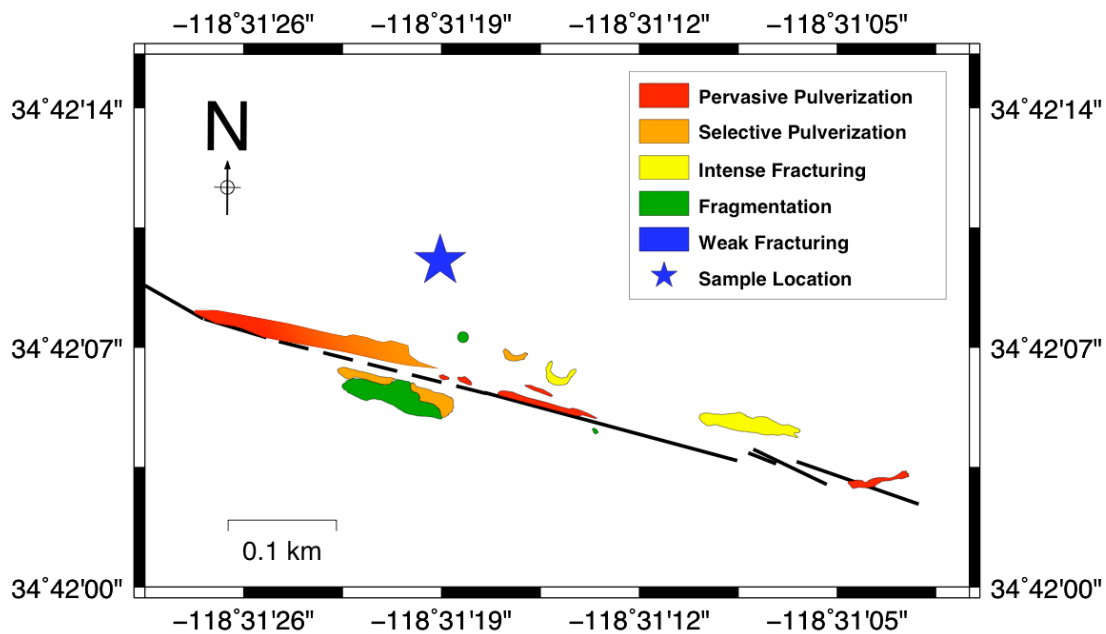
Supplementary figure 2. Sketch of the Split Hopkinson Pressure Bar apparatus. The sample is inserted between two long bars, before being submitted to the stress wave generated by the impact of the “striker”, another bar thrown on the input bar. In the standard SHPB configuration (Kolsky) the strain measured in A shows first a wave induced by the loading (the incident wave) followed by its reflection at the face of the specimen (the reflected wave). The strain measured in B shows a wave induced by the impedance contrast at the specimen (the transmitted wave).



Supplementary figure 3. Experimental results. Each sample was cored from a block. We grouped the samples by block, with one colour for each block. On the left, we show the obtained stress-strain curves. On the right, we reproduce the results of figure 2, using the same conventions as in it: a star denotes a pulverized sample, a filled circle a split sample and an empty square an unbroken sample. Some blocks (red and black) are tougher than others, but the transition lies within the same region of strain rate for all blocks.

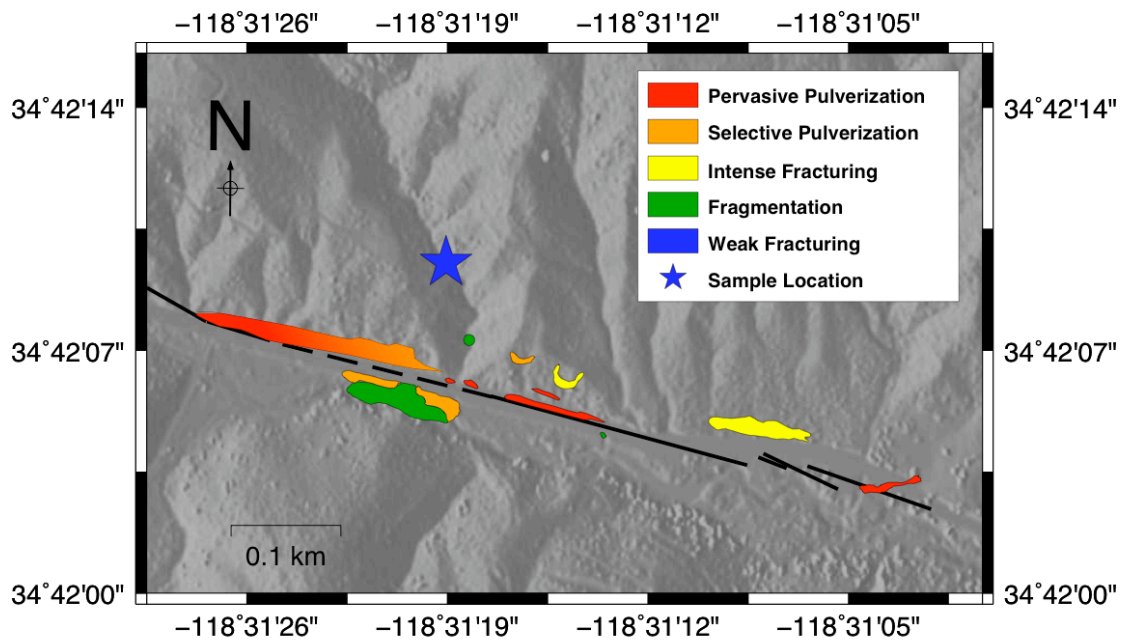


Supplementary figure 4. Maximum shear strain rate $d\varepsilon_s/dt$ versus shear strain ε_s induced by a rupture propagating with a constant below the Rayleigh speed in a location 100 m away from the fault core. We normalized both the strain and strain rate so that the maximum strain amplitude is 2%. The curves were computed for several rupture velocities. All curves achieve a maximum strain rate less than 0.2/s, three orders of magnitude below our experimental 100/s pulverization threshold.



Supplementary figure 5: Location of the samples used in this experiment.

We overlay the pulverization map of (Dor et al, 2006)¹ and the location of the samples (blue star). We use the same color code as in (Dor et al, 2006)¹ : red denotes a pervasive pulverization, when all crystals of the samples can be crushed by hand, orange for selective pulverization when some crystals remains intact, yellow for intense fracturing, when crystals are in the grain size scale, green for fracturing in the centimetre scale. Our sample can be classified as weakly fractured, with only macroscopic large fractures. The map was made using the Generic Mapping Tools (GMT) software²⁸, using a basic cylindrical projection with a central meridian of longitude equal to $-118^{\circ}30'$ and a standard parallel of latitude equal to $34^{\circ}42'$.

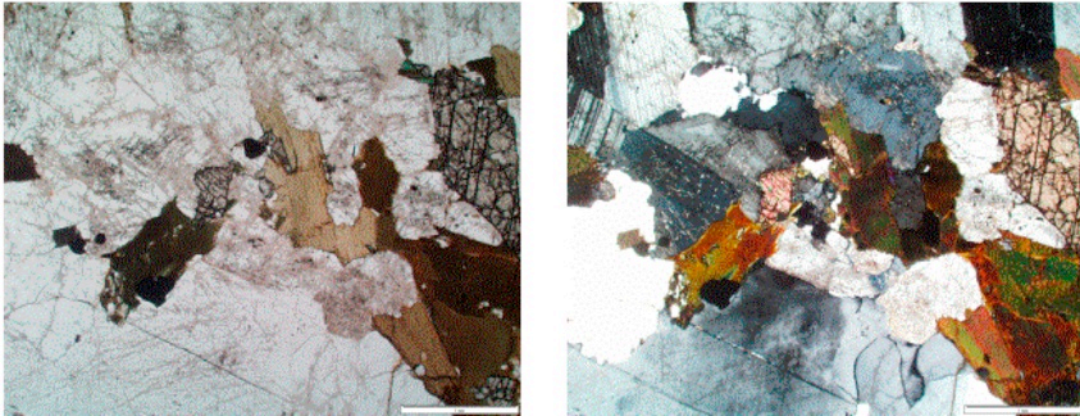


Supplementary figure 6: Location of the samples used in this experiment.

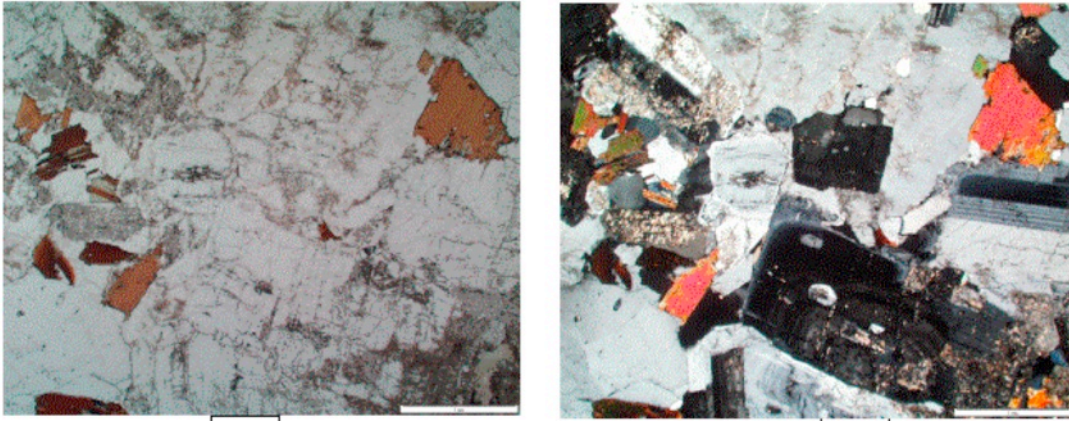
This is the same map as in supplementary figure 5, except that we overlay the topography of the area. The digital elevation data were obtained from the GEON project²⁹. The samples were taken as boulders on the flanks of a deep gully. As they lay above the bottom of the gully, we assume the boulders were not transported by water, but rather that they fell by gravity from the edges of the gully. The flanks are quite steep, so that the originating outcrops could not be investigated.



Supplementary figure 7. Thin section of the granite used to make the samples. Microfractures are highlighted in red. They are easily tracked in quartz but are much less obvious in altered feldspar and soft mica. The thin section is 4.5cm long and 3cm wide.

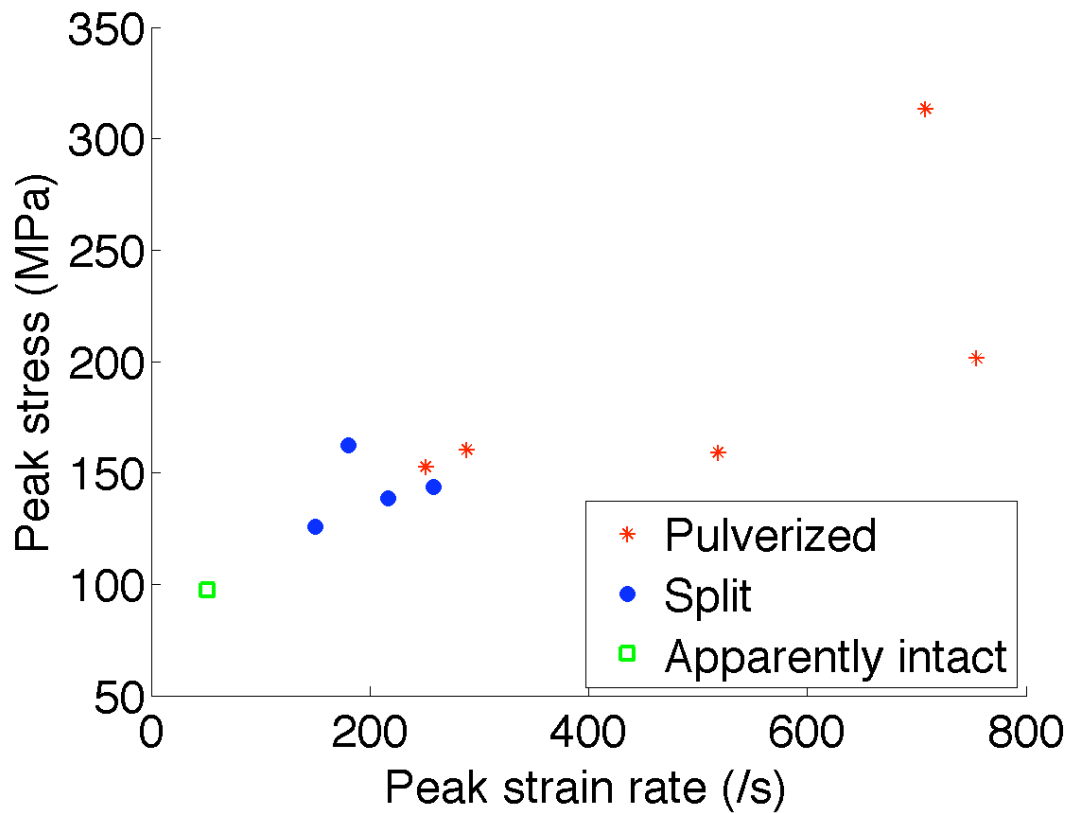


Supplementary figure 8: Thin section of the samples collected near the San Andreas Fault for the experiments. The left image is taken with natural light, and the right image is taken with polarized light. Feldspar is altered. Microfracturing is visible throughout the sample, and is cleared on the minerals with large relief, such as the sphene on the right hand side of the photographs. The scale bar on lower right corner is 1mm long.



Supplementary figure 9: Thin section of the Tarn Granite before testing.

This new set of samples was used for supplementary testing on the sensitivity of the onset of pulverization with initial damage. The scale bar in the lower right corner is 1mm long.



Supplementary figure 10: Transition to pulverization of Tarn Granite. This is the same figure as the figure 2 of the main text, but for intact Tarn Granite samples instead of the damaged San Andreas Fault samples. The transition strain rate is 250/s, instead of 150/s.

Sample	Quartz	K-Feldspar	Plagioclase	Biotite	Amphibole, sphene,...
San Andreas Fault Thin section 1	28.7% [24.5–33.3]	33.3% [28.8 – 38.1]	20.3% [16.5 – 24.5]	16.0% [12.6 – 19.9]	1.6% [0.6 – 3.5]
San Andreas Fault Thin Section 2	28.2% [24.0–32.8]	35.1% [30.7 – 40.0]	19.9% [16.3 – 24.1]	14.9% [11.7 – 18.7]	1.9% [0.8 – 3.8]
Tarn Granite	32.8% [28.4–37.4]	39.4% [34.8 – 44.1]	13.8% [10.6 – 17.4]	14.1% [10.9 – 17.7]	0% [0 – 0.9]

Supplementary Table 1: Modal composition of the rocks tested. Modal analysis was performed by random selection of 105 points of the available thin sections (two for the San Andreas Fault samples, one for the Tarn Granite). 95% confidence interval of the proportion of each mineral (in percent) is given between square brackets below the average composition.

		5D	5I	B5	5H	3E	LHE
Peak strain rate		146/s	143/s	174/s	219/s	260/s	850/s
Peak stress		90MPa	62.5MPa	48MPa	93MPa	83MPa	170MPa
Final state		Fractured	Pulverized	Pulverized	Pulverized	Pulverized	Pulverized
Mass per sieve (g)	>20mm	31.06	0	0	0	0	0
	>16mm	0	0	0	0	0	0
	>12.5mm	0	0	0	1.35	0	0
	>10mm	0	0.86	2.2	0.67	0	0
	>8mm	0	3.76	3.26	1.62	1.48	0
	>6.3mm	0	0.73	3.15	2.84	0.87	1.52
	>4mm	0.24	1.96	3.96	3.49	2.23	3.01
	>2.5mm	0	2.85	2.76	4.69	4.41	6.26
	>2mm	0.06	1.29	1.53	1.48	2.55	1.72
	>1.6mm	0.04	1.06	1.19	0.76	2.37	1.66
	>1.25mm	0.04	0.62	0.7	3.59	1.63	0.95
	>0.8mm	0.01	1.36	1.51	3.61	3.2	1.85
	>0.44mm	0.02	1.07	1.38	3.73	2.56	2.75
	>0.2mm	0.01	0.59	0.75	2.14	1.17	0
<0.2mm	0	0.4	0.63	1.73	0.72	0.63	
Total sieved mass (g)		31.48	16.55	23.02	31.7	23.19	20.35
Initial sample mass (g)		31.65	18.74	23.68	33.44	25.05	21.38
Material loss (g)		0.17	2.19	0.66	1.74	1.86	1.03
Recuperation (%)		99.46	88.31	97.21	94.80	92.57	95.18

Supplementary Table 2: Grain size distribution of the pulverized rocks made from samples from the damaged zone of the San Andreas Fault. The grain size distribution is obtained by manual sieving. We get larger grains than the natural grain size (~100micrometers) observed by (Rockwell et al, 2009)³, but our experiments cannot reproduce the multiple oscillatory loading that the pulverized rocks may have experienced.

		T12	T7	T17	T13	T9
Peak strain rate		180/s	201/s	251/s	288/s	518/s
Peak stress		162MPa	200MPa	153MPa	160MPa	159MPa
Final state		Fractured	Pulverized	Pulverized	Pulverized	Pulverized
Mass per sieve (g)	>10mm	24.37	0	1.98	3.77	0
	>8mm	0	3.67	3.56	3.49	0.76
	>4mm	0.63	5.61	8.02	8.28	10.31
	>2.5mm	0.19	3.72	3.71	2.87	2.73
	>2mm	0.04	1.09	0.62	0.98	1.48
	>1.6mm	0	2	1.39	0.56	1.24
	>1.25mm	0.07	0.92	0.59	0.7	0.94
	>1mm	0	0.82	0.6	0.53	0.67
	>0.8mm	0	1.04	0.57	0.69	0.99
	>0.4mm	0	2.25	1.38	1.13	2.15
	>0.2mm	0	1.92	1.08	0.84	1.55
<0.2mm	0	1.52	0.9	0.54	0.83	
Total sieved mass (g)		25.3	24.56	24.4	24.38	23.65
Initial sample mass (g)		25.33	25.14	25.17	24.94	24.77
Material loss (g)		0.03	0.58	0.77	0.56	1.12
Recuperation rate (%)		99.88	97.69	96.94	97.75	95.48

Supplementary Table 3. Grain size distribution of the pulverized Tarn

Granite samples. The grain size is larger for rock that was initially less damaged.